AEDC-TR-79-65

c. 1

Interagency Nitric Oxide Measurement Investigation: AEDC Results for Phase I (Calibration Technique for Optical Measurement System)

J. D. Few, H. S. Lowry III,
W. K. McGregor, and D. R. Keefer
ARO, Inc.

October 1979

Final Report for Period October 1977 – August 1979

Approved for public release; distribution unlimited.

ARNOLD ENGINEERING DEVELOPMENT CENTER
ARNOLD AIR FORCE STATION, TENNESSEE
AIR FORCE SYSTEMS COMMAND
UNITED STATES AIR FORCE

NOTICES

When U. S. Government drawings, specifications, or other data are used for any purpose other than a definitely related Government procurement operation, the Government thereby incurs no responsibility nor any obligation whatsoever, and the fact that the Government may have formulated, furnished, or in any way supplied the said drawings, specifications, or other data, is not to be regarded by implication or otherwise, or in any manner licensing the holder or any other person or corporation, or conveying any rights or permission to manufacture, use, or sell any patented invention that may in any way be related thereto.

Qualified users may obtain copies of this report from the Defense Documentation Center.

References to named commerical products in this report are not to be considered in any sense as an indorsement of the product by the United States Air Force or the Government.

This report has been reviewed by the Information Office (OI) and is releasable to the National Technical Information Service (NTIS). At NTIS, it will be available to the general public, including foreign nations.

APPROVAL STATEMENT

This report has been reviewed and approved.

Eules L. Hively

EULES L. HIVELY
Project Manager
Directorate of Technology

Approved for publication:

FOR THE COMMANDER

Marion L. Laster

MARION L. LASTER
Director of Technology
Deputy for Operations

REPORT DOCUMENTATION PAGE		READ INSTRUCTIONS BEFORE COMPLETING FORM
1. REPORT NUMBER AEDC-TR-79-65	2. GOVT ACCESSION NO.	3. RECIPIENT'S CATALOG NUMBER
4. TITLE *(and Subtitle)* INTERAGENCY NITRIC OXIDE MEASUREMENT INVESTIGATION: AEDC RESULTS FOR PHASE I (CALIBRATION TECHNIQUE FOR OPTICAL MEASUREMENT SYSTEM)		5. TYPE OF REPORT & PERIOD COVERED Final Report - October 1977 - August 1979 6. PERFORMING ORG. REPORT NUMBER
7. AUTHOR(s) J. D. Few, H. S. Lowry III, W. K. McGregor, and D. R. Keefer, ARO, Inc., a Sverdrup Corporation Company		8. CONTRACT OR GRANT NUMBER(s)
9. PERFORMING ORGANIZATION NAME AND ADDRESS Arnold Engineering Development Center/DOT Air Force Systems Command Arnold Air Force Station, Tennessee 37389		10. PROGRAM ELEMENT, PROJECT, TASK AREA & WORK UNIT NUMBERS Program Element 63723E
11. CONTROLLING OFFICE NAME AND ADDRESS Arnold Engineering Development Center/DOS Air Force Systems Command Arnold Air Force Station, Tennessee 37389		12. REPORT DATE October 1979 13. NUMBER OF PAGES 38
14. MONITORING AGENCY NAME & ADDRESS*(if different from Controlling Office)*		15. SECURITY CLASS. *(of this report)* UNCLASSIFIED 15a. DECLASSIFICATION/DOWNGRADING SCHEDULE N/A

16. DISTRIBUTION STATEMENT *(of this Report)*

Approved for public release; distribution unlimited.

17. DISTRIBUTION STATEMENT *(of the abstract entered in Block 20, if different from Report)*

18. SUPPLEMENTARY NOTES

Available in DDC

19. KEY WORDS *(Continue on reverse side if necessary and identify by block number)*

concentration (chemistry)	ultraviolet spectroscopy	emission control
nitrogen oxide measurements	probes	
gas analyst	computers	
	mathematical models	
	jet engines	

20. ABSTRACT *(Continue on reverse side if necessary and identify by block number)*

As part of the continuing investigation to determine the cause of the differences that were formerly found to exist between nitric oxide (NO) concentrations measured with conventional sample extraction-gas analyzer techniques and with an ultraviolet (UV) spectroscopic technique, an experimental program was undertaken at United Technologies Research Center (UTRC) Facility, East Hartford, Connecticut. The purpose of Phase 1 of this program was

DD FORM 1 JAN 73 1473 EDITION OF 1 NOV 65 IS OBSOLETE

20. ABSTRACT (Continued)

to measure NO concentrations in several sources with known amounts of NO and over the range of temperatures from 300 to 2,000 K. Spectroscopic and probe measurements were obtained and compared over the test envelope. During this period, a discrepancy in the NO computer model (developed at AEDC) used for reducing the data was identified and has since been corrected. Included in this report are the results of the optical measurements, a comparison of these results with the known concentrations, and a description of the new computer model.

AFSC
Arnold AFS Tenn

PREFACE

The work reported herein was conducted by the Arnold Engineering Development Center (AEDC), Air Force Systems Command (AFSC), at the request of the Air Force Engineering and Service Center, Tyndall Air Force Base, Florida. The results of the research were obtained by ARO, Inc., AEDC Division (a Sverdrup Corporation Company), operating contractor for the AEDC, AFSC, Arnold Air Force Station, Tennessee, under ARO Project Numbers E34P-R4A and P34I-02A. The data analysis was completed on June 4, 1979, and the manuscript was submitted for publication on August 20, 1979. The Air Force project managers were Capt. Harvey Clewell, of Tyndall Air Force Base, and E. L. Hively, Directorate of Technology, AEDC. The experimental phase was conducted at the United Technologies Research Center Facility in East Hartford, Connecticut.

The authors wish to express their appreciation to M. F. Zabielski, L. G. Dodge, and M. Colket, UTRC, for their cooperation and dedication during the experimental phase of this program. In addition, the authors gratefully acknowledge the assistance provided by W. E. Myers, ARO, Inc., from system buildup through data acquisition.

CONTENTS

ILLUSTRATIONS

Figure Page

TABLES

APPENDIX

1.0 INTRODUCTION

Differences between measurements of nitric oxide (NO) emissions from combustion sources using conventional sample extractor techniques and those using an *in situ* ultraviolet (UV)-absorption (optical) technique have been reported (Refs. 1, 2, and 3). The Federal Aviation Administration (FAA) is directing an Interagency-sponsored program to determine the cause of the differences found between the measurements using the two techniques. As part of this investigation, United Technology Research Center (UTRC) has provided several combustion sources to evaluate the differences between the optical and probe techniques (Ref. 4). Arnold Engineering Development Center (AEDC) personnel have made measurements using the UV-absorption technique (developed at AEDC) at the UTRC facility in East Hartford, Connecticut, and the results of the first phase of that study are reported.

The Interagency NO Investigation has three major tasks. Task 1 is the development of calibration techniques for the optical measurement systems; Task 2 emphasizes determining the relevant chemistry occurring in the sample extraction and in the transfer lines to the NO measurement instrumentation; Task 3 includes both optical and probe sampling on three progressively more complicated combustion systems. UV-absorption measurements will also be made by UTRC using basically the same approach as that used by AEDC, and an infrared correlation technique is also used (Ref. 4). The results of all measurements, both probe and optical, will be compared and analyzed.

This report summarizes the results of measurements made by AEDC during the optical calibration phase (Task 1) of the overall program. During the Task 1 phase, some discrepancies were identified by UTRC personnel (Ref. 4) in the original theoretical optical-transmission model developed at AEDC for nitric oxide concentration measurements. The model has since been corrected by AEDC/ARO personnel; a review of the theory is included in this report. (UTRC has also developed its version of the model, which is described in Ref. 4.) Model predictions are compared to data points obtained from the UTRC calibration cell, flowing-gas heater, and flat-flame burner. These data points span the temperature range from 300 to 1,750 K at a pressure of 1 atm. Agreement of the optical measurements with calculated inputs of NO concentration in conjunction with probe profiles is generally within the uncertainty of the probe measurements.

2.0 REVIEW OF MODEL

2.1 THEORY

A theoretical model for the transmission of Doppler-broadened resonance line radiation through absorbing media with combined Doppler and pressure broadening was given by Davis, McGregor, Few, and Glassman (Ref. 5) with application to the γ band of NO. As shown by Ref. 4, the formulation given in Ref. 5 was incorrect in that Hund's case (b) statistics (Ref. 6) were used, the spin splitting was not properly taken into account, and the normalization of the line oscillator strength was inconsistent with the literature (Refs. 7 and 8). The method of calculation of the partition function in the model has now been changed to conform to the angular momentum coupling intermediate between Hund's cases (a) and (b) in accordance with Keefer (Ref. 9) and as discussed in Ref. 4. A brief review of the theory is presented in the following.

The transmission, t, of an isolated, Doppler-broadened emission line through a homogeneous medium of length, ℓ, is given by

$$t_j = I^{0}_{\nu_j 0} \int_0^{\infty} \exp \left\{ - \left[\frac{2\left(\nu - \nu_j^0\right)}{\left(\Delta_s \nu_j\right)_D} \sqrt{\ln 2} \right]^2 \right\} \exp \left[-k(\nu)\, \ell \right] d\nu \tag{1}$$

where $I^{0}_{\nu_j 0}$ is the intensity of the source line at line center, ν_j^0 is the frequency at line center, $(\Delta_s \nu_j)_D$ is the half-width of the Doppler-broadened line, and $k(\nu)$ is the monochromatic absorption coefficient of the medium. The half-width of the source line depends on the source temperature and is given by

$$\left(\Delta_s \nu_j\right)_D = 2\nu_j^0 \sqrt{\frac{2 \ln 2\, \kappa T_s}{M_s c^2}} \tag{2}$$

where M_s is the molecular weight of the emitting molecule, T_s is the source temperature, κ is Boltzmann's constant, and c is the speed of light.

The absorption coefficient, $k(\nu)$, contains contributions, $k_i(\nu)$, from all lines near the frequency, ν_j^0. Each of these lines will be broadened both by the Doppler effect and by collisions. The absorption coefficient of the ith line is given by the Voigt profile,

$$k_i(\nu) = k_i^0 \frac{1}{\pi} \int_{-\infty}^{\infty} \frac{\mathfrak{a} e^{-y^2}}{\mathfrak{a}^2 + (\omega_i - y)^2} dy \tag{3}$$

where k_i^0 is the centerline Doppler absorption coefficient of the i^{th} line, and the broadening parameter, $\mathfrak{a}$, is a parameter proportional to the ratio of the collision-broadened half-width, $(\Delta_a \nu_i)_L$, to the Doppler-broadened half-width, $(\Delta_a \nu_i)_D$, in the absorbing medium. The broadening parameter, $\mathfrak{a}$, equation is as follows:

$$\mathfrak{a} = \frac{(\Delta_a \nu_i)_L}{(\Delta_a \nu_i)_D} \sqrt{\ln 2} \tag{4}$$

The parameter ω_i in Eq. (3) is the Doppler function

$$\omega_i = \frac{2(\nu - \nu_i^0)}{(\Delta_a \nu_i)_D} \sqrt{\ln 2} \tag{5}$$

It can be shown (Appendix A and Ref. 10) that for binary collisions

$$\mathfrak{a} = C\, p/T \tag{6}$$

where p is the pressure, T is the temperature, and C is a constant which, for any given mixture of broadening species, b, of mass, M_b, mole fraction, f_b, and broadening-collision cross section, σ_{ab}, is given by

$$C = \frac{\lambda}{\kappa \pi^{3/2}} \sum_{b} f_b \sigma_{ab} \left(1 + \frac{M_a}{M_b}\right)^{1/2} ; \sigma_{ab} = \pi d_{ab}^2 \tag{7}$$

where λ is the wavelength and d_{ab} is the optical diameter. The appropriate absorption coefficient in Eq. (1) must include the contributions due to all absorbing lines that overlap the source line, j; thus,

$$k(\nu) = \sum_{i} k_i(\nu) = \sum_{i} \frac{k_i^0}{\pi} \int_{-\infty}^{\infty} \frac{\mathcal{G} e^{-y^2}}{\mathcal{G}^2 + (\omega_i - y)^2} \, dy \tag{8}$$

There may be several emission lines within a given instrument bandpass, $\Delta\nu_I$. The contributions of each of these lines must be summed to obtain the transmission within the given instrument bandpass. Thus, the transmissivity within the bandpass, $\Delta\nu_I$, is given by substitution of Eq. (8) into Eq. (1), summing over the emission lines, j, and dividing by the total intensity of the source within the bandpass as follows:

$$\tau_{\Delta\nu_I} = \frac{\sum_{j} I_{\nu_j^0}^0 \int_{\Delta\nu_I} \exp\left\{-\left[\frac{2(\nu - \nu_j^0)}{(\Delta_s \nu_j)_D} \ell n\, 2\right]^2\right\} e^{-\ell k(\nu)} \, d\nu}{\sum_{j} I_{\nu_j^0}^0 \int_{\Delta\nu_I} \exp\left\{-\left[\frac{2(\nu - \nu_j^0)}{(\Delta_s \nu_j)_D} \ell n\, 2\right]^2\right\} d\nu} \tag{9}$$

where $k(\nu)$ is given by Eq. (8).

The line center absorption coefficient for a single transition out of the 12 possible transition from a given J″ is given (Ref. 5) by

$$k_i^0 = \left(\frac{2e^2 \sqrt{\pi \ell n\, 2}}{m_e c^2}\right) \frac{N(v''J''K''p)\, f(n'v'J'K'n''v''J''K'')}{(\Delta_a \nu_i)_D} \tag{10}$$

where i refers to the particular n′v′J′K′n″v″J″K″ transition in the $A^2\Sigma \rightarrow x^2\Pi$ γ-band system of NO. The constants in parenthesis are the electron charge, e, the electron mass, M_e, and the speed of light, c,. The population of the v″ vibrational level in the J″K″ rotational sublevel and one of the parity levels, p, (+ or -) of the $^2\Pi_\Omega$ state in the intermediate angular momentum coupling case between Hund's cases (a) and (b) is given (Ref. 9) by

$$\frac{N(v''J''K''mp)}{N_{total}} = \frac{(2J''+1)\exp\left\{\frac{-G(v'')+F_m(J'')}{\kappa T}\right\}}{2\sum_v\left\{\exp\left[\frac{-G(v)}{\kappa T}\right]\sum_{m=1}^{2}\sum_{J=\Omega_m}^{\infty}(2J+1)\exp-\left[\frac{F_m(J)}{\kappa T}\right]\right\}} \tag{11}$$

where T is the temperature, G(v″) is the vibrational energy (cm^{-1}). $F_m(J'')$ is the rotational energy (cm^{-1}) for either the $^2\Pi_{1/2}$ state (m = 1) or the $^2\Pi_{3/2}$ state (m = 2) and for purposes of the population calculation is approximated by the Hill and Van Vleck formulas (Ref. 6)

$$F_1 = B_v\left[\left(J+\tfrac{1}{2}\right)^2 - 1 - \tfrac{1}{2}\sqrt{4\left(J+\tfrac{1}{2}\right)^2 + Y(Y-4)}\right] - D_vJ^4 \tag{12a}$$

$$F_2 = B_v\left[\left(J+\tfrac{1}{2}\right)^2 - 1 + \tfrac{1}{2}\sqrt{4\left(J+\tfrac{1}{2}\right)^2 + Y(Y-4)}\right] - D_v(J+1)^4 \tag{12b}$$

where $Y = A/B_v$ where A is the splitting constant, B_v is the inertial rotational constant, and D_v is the contrifugal rotational constant. The oscillator strength for the transition is given by

$$f(n'v'J'K'n''v''J''K'') = \frac{S(J'K'J''K'')}{2J''+1}\,\frac{\nu(J'K'J''K'')}{\nu(v'v'')}\,f(v'v'') \tag{13}$$

where $\nu(J'K'J''K'')$ and $\nu(v'v'')$ are the frequencies of the line and band centers and where the normalization for the Honl-London factor S(J′K′J″K″) and the normalization of the band oscillator strength follow that of Tatum (Ref. 7) and are consistent with Pery-Thorne and Banfield (Ref. 8). The Honl-London factors are those of Earls that had been defined earlier (Ref. 5).

The line positions, ν_j^0, previously used were those of Deezi (Ref. 11). Improved data have recently become available (Ref. 12), and these data have been correlated by UTRC (Ref. 4) into a consistent formulation. These new line positions have been incorporated into the AEDC model.

The source parameters are the peak line intensity, $I_{\nu_j}^{0_0}$, and the Doppler half-width of the lines, $(\Delta_s \nu_j)_D$. It is sufficient to determine only the relative peak line intensity since any absolute magnitude will cancel in Eq. 9. The relative peak line intensity can be determined by direct measurement for resolved lined; the intensities of the unresolved lines can be determined from the upper state population implied by the measured line intensities. However, for low-pressure, Doppler-broadened source lines in the ultraviolet, direct measurement of either the half-width or the source temperature is difficult. Section 2.2 describes an indirect method of determining source temperature.

The absorber parameters are the absorption coefficient at line center, k_i^0, and the quantity $\mathfrak{C}$, related to the collisional broadening. If the temperature and density within the absorption path are known, then k_i^0 is determined by Eq. (11) if the band oscillator strength, $f(v'v'')$, is known. Thus, when k_i^0 is known, the broadening coefficient, C, of Eq. (6) can be determined from the value of broadening parameter, $\mathfrak{C}$, required to obtain a match between the measured transmissivity and the transmissivity calculated from the model based on Eqs. (9) through (13).

Successful application of the model represented by Eqs. (9) through (13) requires a known source line intensity distribution, source temperature, band oscillator strength, and broadening coefficient.

2.2 PARAMETERS

The model represented by Eqs. (9) through (13), together with carefully controlled laboratory experiments, can be used to determine the source temperature, T_s, and the broadening parameter, $\mathfrak{C}$, when the source line positions and intensities are specified and the band oscillator strength is known. Careful measurements of oscillator strength have been made for the NO molecule using several methods (e.g., Refs. 8, 13, and 14). Review of these measurements shows the value of $4.09 \pm 0.1 \times 10^{-4}$ of Hassan et al. (Ref. 13) for the oscillator strength of NO to be the most reliable.

2.2.1 Source Lines

The line positions of the (0,0) band of the γ system of NO as specified by Ref. 4, interpreting Engleman's data (Ref. 12), have been adopted as the most accurate available.

The source line intensity distribution of the AEDC capillary discharge lamp has been remeasured with resolution sufficient to identify many lines lying in each of the independent branches of the (0,0) band. No changes from the previously reported intensity distribution (Ref. 5) were found. It should be noted that the line discharge lamp and its operating conditions (pressure, gas mixture, and voltage applied) and different designs (e.g., hollow cathode configuration as used in Ref. 4) would be expected to exhibit a different distribution. Furthermore, there is no reason to expect the intensity distribution to follow a Boltzmann distribution of the population because of the complex excitation mechanism within the electrical discharge.

2.2.2 Source Temperature

Determination of the effective source temperature hinges on the fact that at low pressure the transmissivity becomes independent of the other unknown parameter, the collision-broadening parameter. In the low-pressure limit, the combined Doppler- and collision-broadened absorption profile [Eq. (3)] reduces to a Gaussian profile whose half-width depends only upon the absorber temperature. Thus, if the absorber temperature and number density are known, and the measured value of oscillator strength is used, the only unknown in Eq. (9) is the Doppler half-width of the source. This half-width is directly related to the source temperature through Eq. (2).

The experimental apparatus described in Ref. 5 was used to make a carefully controlled set of transmission measurements. A sequence of transmissivity measurements at the second bandhead was made over a range of pressures, with the NO number density and temperature held constant. In order to determine the source temperature, the transmissivity for a given number density and temperature was determined from the intercept of the transmissivity versus pressure curve (Fig. 1) in the limit of zero pressure (corresponding to $\mathfrak{A} = 0$). This value of transmissivity was used together with Eq. (9) in the limit where $\mathfrak{A}$ approaches zero to determine the source temperature by adjusting source temperature to force a match between the calculated and extrapolated, measured transmissivities. A value of source temperature of 950 ± 25 K was obtained by this exercise. Again, it should be noted that the source temperature is a characteristic of the lamp design and is expected to vary for different designs.

2.2.3 Broadening Coefficient

Once the source temperature has been determined, the only unresolved parameter in Eq. (9) is $\mathfrak{A}$, the parameter proportional to the ratio of collision- to Doppler-broadening half-widths.

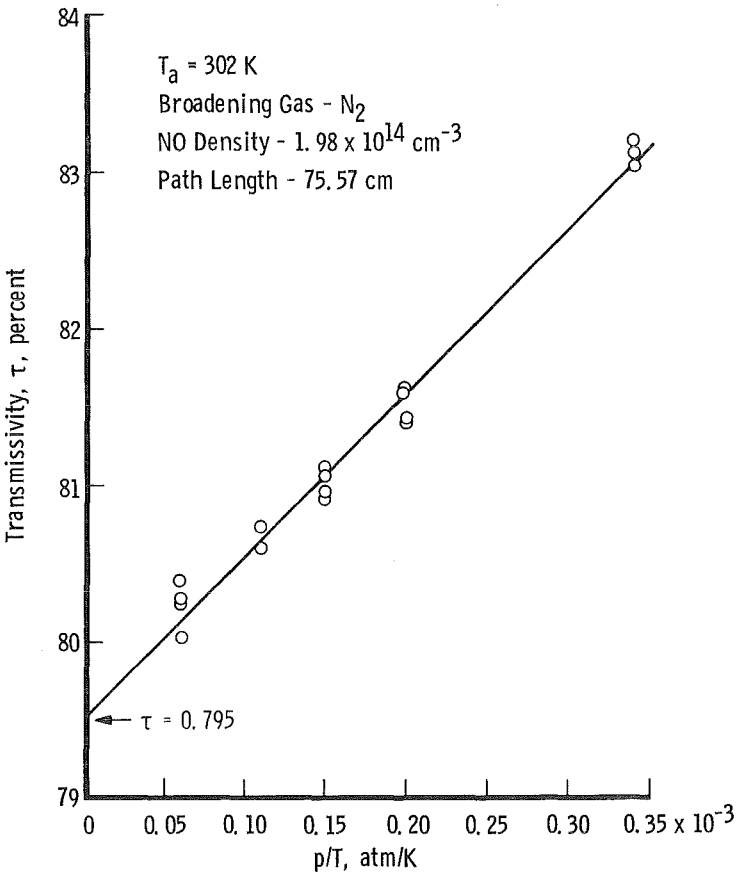

Figure 1. Least-squares fit to measured transmissivity versus p/T.

A series of experiments was performed for known concentrations of NO and various diluent gases over a range of pressures from 15 to 760 torr. The measured values of transmissivity—together with Eqs. (9) through (13)—were used to determine the value of α for each experimental condition. A least-squares curve fit to these data was used to determine the value of C in Eq. (6), and the broadening cross section was determined from Eq. (7). Since the calibration gas was a mixture of NO in N_2, the coefficient, C, for both Ar and Co_2 was determined by use of Eq. (7). Figure 2 is a plot of α versus p/T for some 100 data points using N_2 as the broadening gas and showing the least-squares straight line fit to the data. The results for the broadening of No by N_2, A, and CO_2 are given as follows:

Collision Partner	C, $\frac{k}{atm}$	Cross Section, 10^{-16} cm^2	Collision Diameter, A°
N_2	2,390 ± 220	556 ± 53	13.3 ± 0.6
A	2,150 ± 200	547 ± 53	13.2 ± 0.6
CO_2	2,090 ± 200	540 ± 53	13.1 ± 0.6

It should be noted that at the higher pressures where the absorbing lines are considerably broader than the source lines, the transmissivity becomes relatively independent of the source temperature determined from the low-pressure measurements. However, at intermediate pressures, where source line width and absorber line width are comparable, the correct source temperature is essential for an accurate determination of the collision-broadening parameter by the method used here.

The magnitude and the near-constant value of the collisional cross section for broadening of NO γ-band lines by the three molecules studied suggest that long-range electronic forces are responsible for the broadening and that motion of the nuclei is not affected. For data reduction in the UTRC experiments, the following equation was used

$$C = C_o \sum_b f_b \left(1 + \frac{30}{M_b}\right)^{1/2} \tag{14}$$

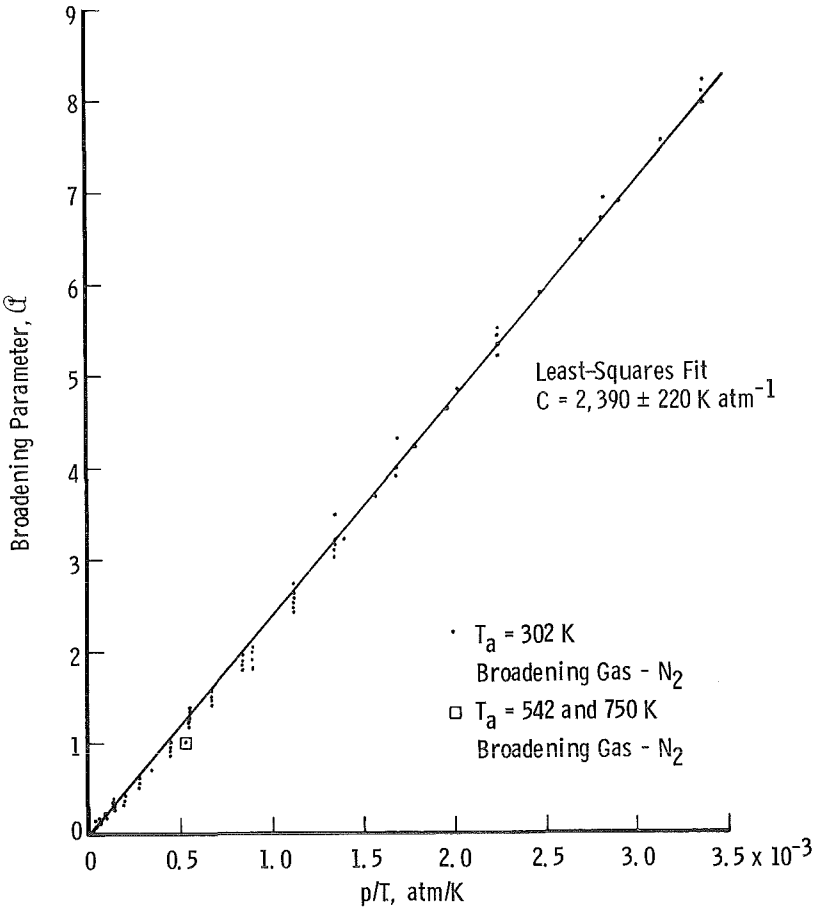

Figure 2. Values of the spectral broadening parameter, ℭ , as a function of p/T for the (0,0) γ band of NO.

where C_o = 1,656 K/atm from the measurements reported here. It should be emphasized that Eq. (14) when applied to other gases represents an assumption. For the UTRC experiments, gases of interest are N_2, A, H_2o, and O_2. Thus C for H_2O and O_2 are assumed to follow Eq. (14) purposes of data reduction.

2.2.4 Model Reproducibility

If the source line intensity distribution, source temperature, oscillator strength, and collision diameter have all been correctly determined, the model should accurately predict the transmissivity over the complete pressure and temperature range covered by the measurements. In Fig. 3 the model represented by Eqs. (9) through (13), using the parameters determined as described above, is compared to the laboratory transmissivity measurements at the second bandhead over the pressure range from 15 to 760 torr for an absorption cell density of 2.14×10^{14} cm^{-3} at room temperature. The model was also checked successfully using a wide range of other absorption cell data taken before and after the UTRC measurement program. The standard deviation for all points of Fig. 3 is ± 0.5 percent. This agreement between predicted and measured transmissivity over a large pressure range indicates the accuracy of the current AEDC model and the correct determination of the model parameters within the pressure and temperature ranges used in the laboratory. It is also noteworthy that the model now predicts the first bandhead transmissivity accurately, contrary to the previous model.

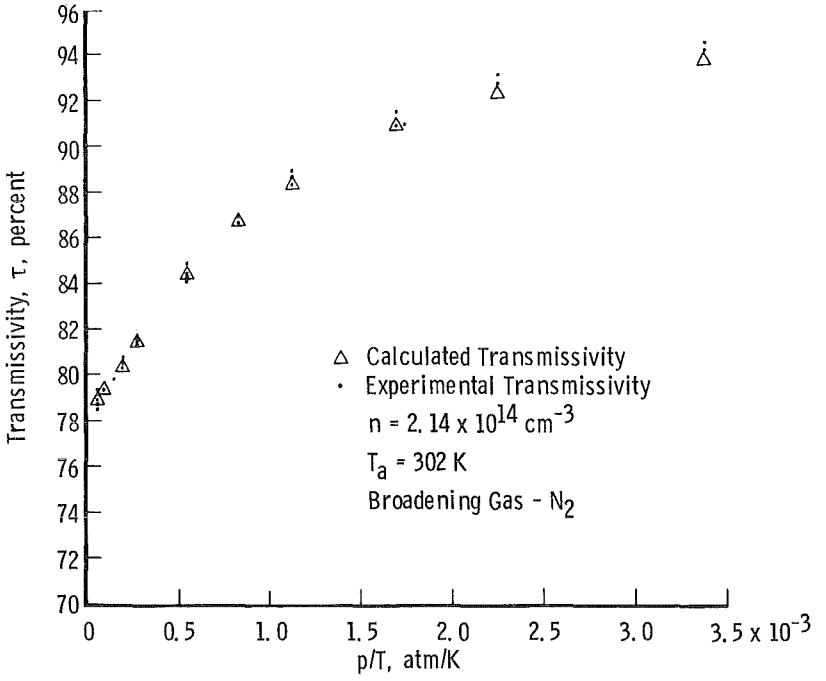

Figure 3. Experimental measured transmissivity compared to model predicted transmissivity.

3.0 OPTICAL CALIBRATION RESULTS

3.1 UTRC CALIBRATION SOURCES

The UTRC high-temperature calibration system (flowing-gas heater and flat-flame burner) is described fully in Ref. 4. It was designed to minimize both gas phase and surface reactions by using argon as the carrier gas in the heater system and as a diluent in the lean H_2/O_2 flat-flame burner. Also, under these conditions the loss of NO in probes should be minimized because of the lack of hydrocarbons and free hydrogen in the high-temperature gas flow, the agents suspected to be responsible for the NO-destroying probe reactions (Ref. 15). Therefore, comparison between probe and optical results should provide a reasonable calibration for the optical technique. A static absorption cell (Ref. 4) was also used to provide a datum for optical measurements by all parties. These three sources—static absorption cell, flowing-gas heater and flat-flame burner, and optical system—will be described briefly in this report.

3.1.1 Static Absorption Cell

The static cell was a stainless steel pipe 18.6 cm in length by 2.03 cm in diameter with quartz windows at either end. A gas mixing and filling system described in Ref. 4 permitted evacuation of the cell and filling with calibration gas to a known pressure and NO concentration. The cell was operated at room temperature.

3.1.2 High-Temperature Calibration Facility

The high-temperature calibration facility housed either the flowing-gas heater (FGH) for temperatures up to 1,000 K, or the flat-flame burner (FFB) for temperatures up to 2,000 K. A rectangular, water-cooled, stainless-steel shroud 22 cm by 14 cm and 26 cm high prevented atmospheric entrainment and contained the hot gas flow which was exhausted through a vent system to the outside of the building. The FGH or the FFB sources were mounted inside the shroud at the base of the rectangular duct. A gas-mixing and metering system supplied the desired gases to the sources. Viewing ports, 3.4 cm in internal diameter (ID) by 10.4 cm in length, with optical windows mounted at either end provided a viewing path through the center of the shroud along the 22-cm path. After the problem of calibration gas buildup within the view tubes was encountered, a purge of dry nitrogen was introduced just inside the optical windows.

Flowing-Gas Heater—A quartz bead bed is heated through radiation from electrically powered ceramic heating units to the desired temperature. Metered calibration gas diluted

with either N_2 or A flows through the quartz bed and is heated by contact with the quartz surfaces. The calibration gas flows through a 17.4- by 9.2-cm (158.3-cm^2)-area quartz duct into the rectangular shroud. The calibration gas is surrounded by a narrow sheath of buffer gas, N_2, which has a temperature near that of the calibration gas. The stream overall NO concentration is controlled by the metered flow. The concentration and temperature profiles are influenced by the optical port purge gas, by normal mixing with the external stream, and by the heater characteristics (Ref. 4). The stream temperature and concentration profiles along the optical path were measured by UTRC using sampling and thermocouple probes located a distance of 4.0 cm above the heater exit plane. The optical axis was also located at a distance of 4.0 cm above the exit plane.

Sampling probes of various designs were used to access different portions of the optical path. (The standard probe was too large for the area near the stream edges.) The probes are described in Ref. 4. Sample line measurements were made using either a chemiluminescent analyzer or a mass spectrometer, the majority of the measurements made by the latter. Concentration profiles provided by UTRC to correspond to the optical measurements are shown in Figs. 4 and 5. The profiles are identified by profile designation in Table 1 with a particular optical measurement. The profiles are shown normalized to values determined by the gas-metering system. The available probe measurements for the centerline are also given in Table 1.

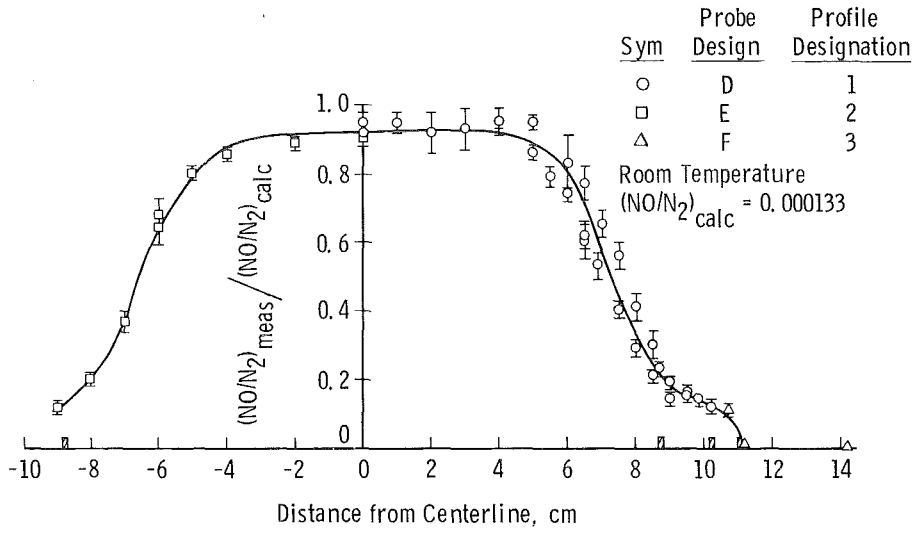

Figure 4. Normalized NO concentration profiles of the flowing-gas heater at room temperature.

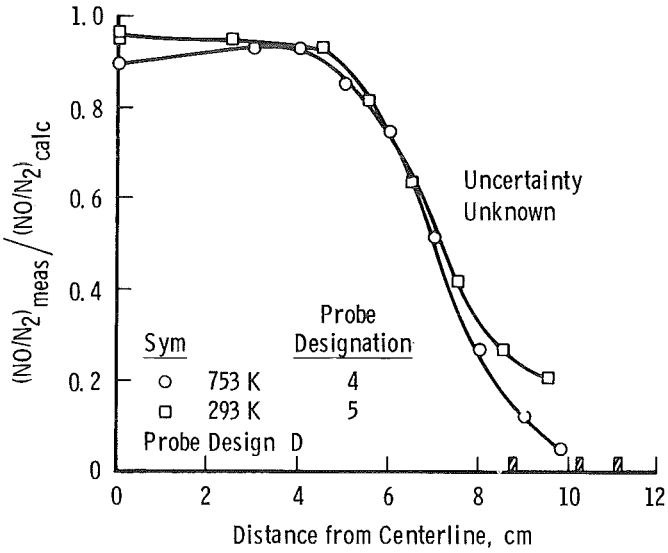

Figure 5. Normalized NO concentration profiles of the flowing-gas heater at elevated temperature.

The gas temperature profiles along the optical path for the FGH were obtained by a Chromel®-Alumel® thermocouple probe (0.010-in.-diam wire and 0.015-in.-diam junction). These profiles are shown on Fig. 6 for the data points indicated in Table 1. Radiation corrections were not made to these data because they were thought to be negligible (Ref. 4). The nominal temperature for each data point is given in Table 1. The nonuniformity in the temperature profile has been attributed by UTRC to transient conditions in the heater; these conditions are peculiar to the particular data points listed.

Table 1. Operating Conditions for Flowing-Gas Heater

Data Point Number	Temperature Profile Used	Average Temperature, K	Concentration Profile Used	Centerline NO Concentration, ppm		Diluent Gas
				Metered	Probe	
2	---	293	1,3	115	---	A
8	---	293	1,3	115	112	N_2
9	---	293	1,3	301	287	N_2
11	6	467	5	115	---	A
12	6	467	5	301	---	A
14	6	453	5	115	---	N_2
15	6	448	5	301	---	N_2
17	6	423	5	301	---	N_2
19	8	833	5	115	105	N_2
20	7	793	5	301	280	N_2
23	7	788	5	115	---	A
24	7	793	5	301	---	A
27	8	823	5	535	520	A
28	8	828	5	448	430	N_2

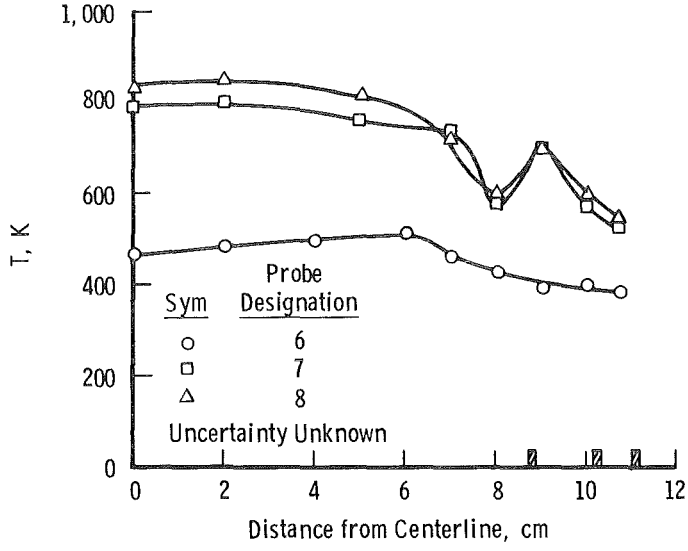

Figure 6. Temperature profiles of the flowing-gas heater

Flat-Flame Burner—The flat-flame burner consisted of a lean burning H_2/O_2 premixed porous-plate burner in which NO and A calibration gases were mixed. Mixture contents in the form of mole fractions are given for each optical measurement point in Table 2. The interior of the rectangular burner measures 17.5 by 9.2 cm (161 cm^2). A surrounding buffer gas (area 76 cm^2) of lean burning H_2/O_2 and argon was also supplied.

The gas sampling of the flat-flame burner at a distance of from 1 to 2 cm (depending on the data point) from the burner face was accomplished in the main part of the flow by water-cooled quartz probes. Near the wall (less than 1.5 cm) an uncooled quartz probe was used. Concentration profiles for the optical data points given in Table 2 are shown, normalized to the value obtained from the gas-metering system, in Figs. 7 and 8. Centerline values obtained from both the gas-metering system and from probes are also given in Table 2. The spread in concentration shown in Fig. 8 is attributed by UTRC to uncertainty in the mass spectrometer measurements (Ref. 4).

The temperature profiles for the FFB were measured using a buttwelded Ir/60% Ir/40% Rh thermocouple (0.003-in.-diam wires) coated with a mixture of 10% beryllium oxide and 90% yttrium oxide. Radiation corrections were made using the thermal balance approach outlined in Ref. 4. The temperature profiles along the optical path for the FFB are shown in Figs. 9 through 12. The radiation correction shown on Figs. 9 through 12 amounts to as much as 200 K; Ref. 4 estimates the error in the correction at 25 to 40 percent.

Table 2. Operating Conditions for Flat-Flame Burner

Data Point Number	Temperature Profile Used	Average Temperature, K	Concentration Profile Used	Centerline NO Concentration, ppm		Argon Mole Fraction Cal.	H_2O Mole Fraction Cal.	Distance From Burner Face, cm
				Metering	Probe			
7	16	1,755	Avg.	1,390	1,427	0.5836	0.414	1.0
10	13	913	12	1,394	1,486	0.8596	0.0678	2.0
13	14	1,278	10	1,362	1,459	0.8240	0.1097	1.5
16	13	913	12	1,076	---	0.8592	0.0680	2.0
17	13	913	12	686	---	0.8593	0.0682	2.0
20	14	1,278	10	1,052	1,119	0.8236	0.1101	1.5
21	14	1,278	10	670	---	0.8234	0.1105	1.5
24	15	1,474	Avg.	1,000	1,107	0.7825	0.1827	1.5
25	15	1,474	Avg.	1,141	---	0.7828	0.1824	1.5
26	15	1,474	Avg.	750	---	0.7820	0.1831	1.5
27	15	1,474	Avg.	607	---	0.7819	0.1832	1.5
30	16	1,755	Avg.	1,584	1,671	0.5842	0.4133	1.0
33	---	293	9	301	---	1.00	---	1.0
34	---	293	9	214	---	1.00	---	1.0
35	---	293	9	115	---	1.00	---	1.0

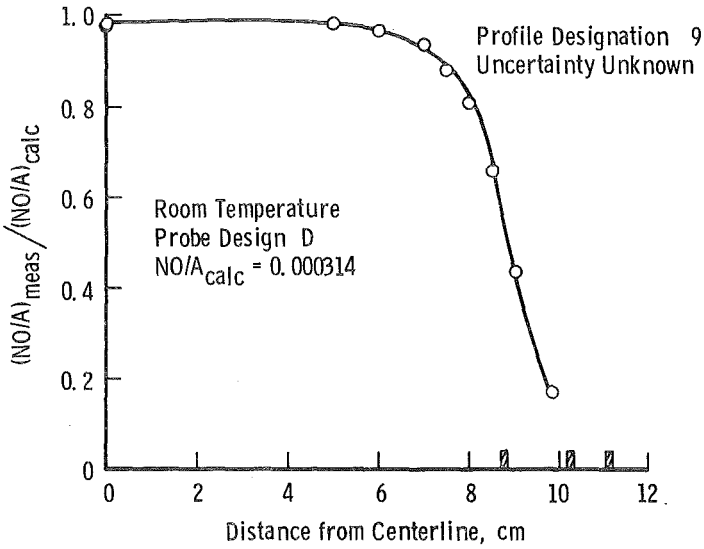

Figure 7. Normalized concentration profiles of the flat-flame burner at room temperature.

Sym	Mass Spectrometer	Centerline ppm, NO	Profile Designation
○	1,220 K (Uncorrected)	1,995	10
□	950 K (Uncorrected)	2,030	11
△	950 K (Uncorrected)	---	12

X^{o}_{NO} - from Flow Calculations
Probe Design B

-- Extrapolation from known zero concentrations of NO(C/A) in the purge ports and from similar measurements on the FGH.

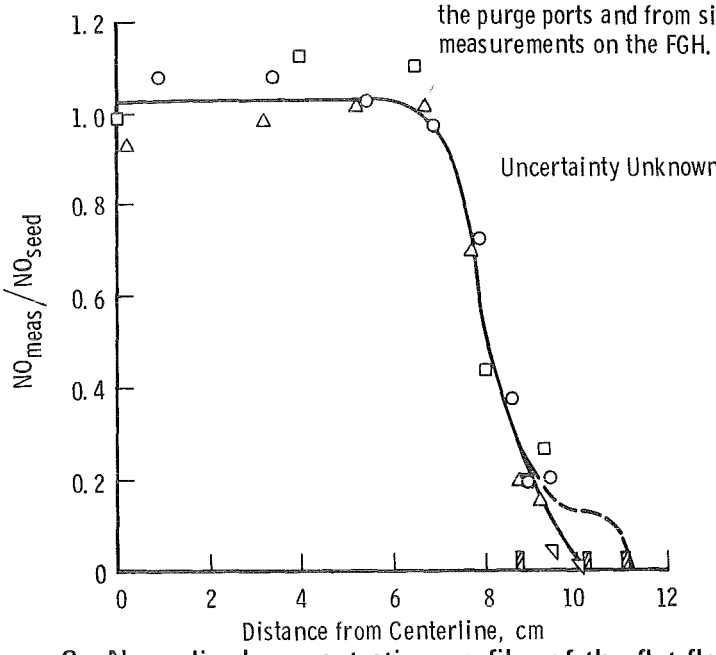

Figure 8. Normalized concentration profiles of the flat-flame burner at elevated temperature.

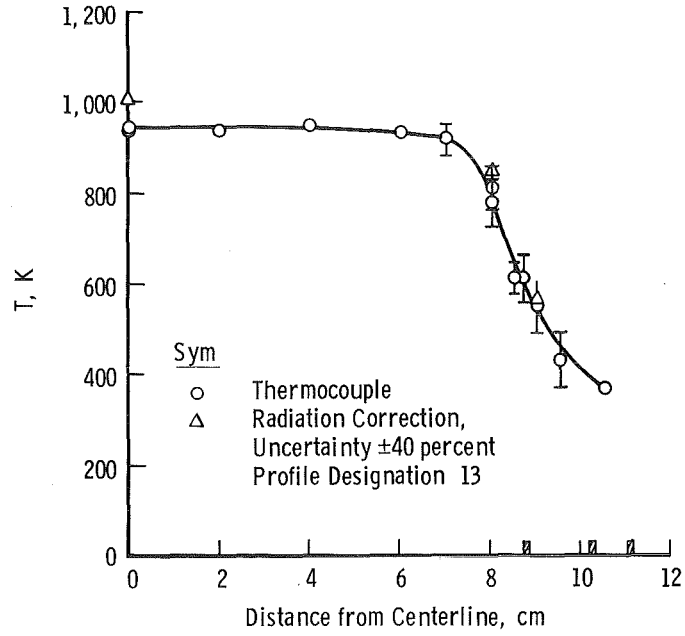

Figure 9. Temperature profile of the flat-flame burner (1,000-K setting).

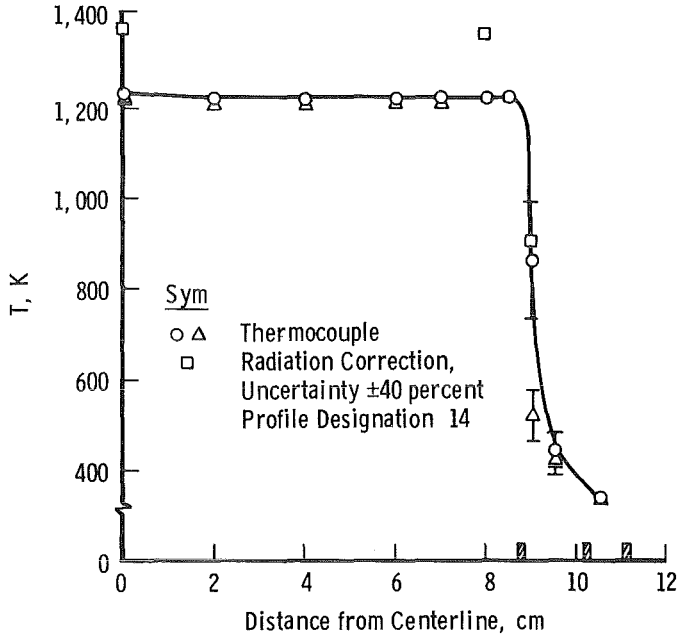

Figure 10. Temperature profile of the flat-flame burner (1,500-K setting).

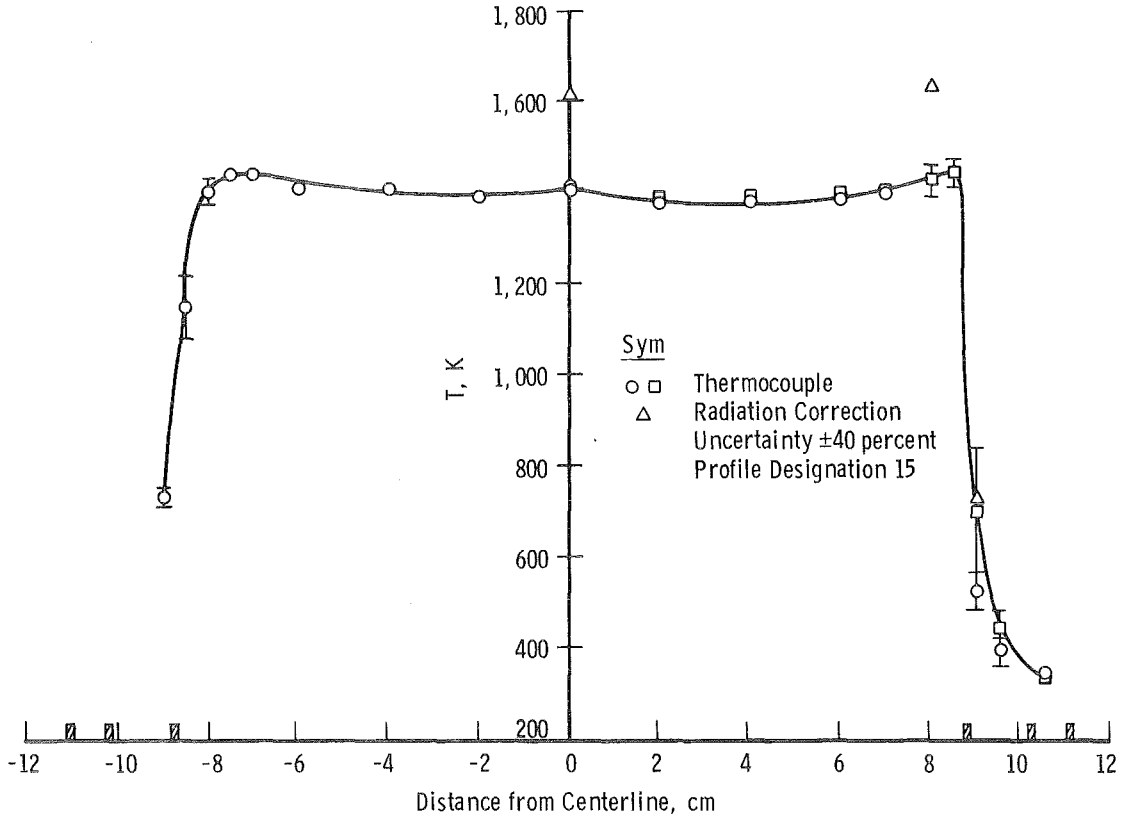

Figure 11. Temperature profile of the flat-flame burner (1,750-K setting).

3.2 AEDC OPTICAL SYSTEM AND MEASUREMENTS

The AEDC UV Resonance Absorption System used for the UTRC measurements consisted of a capillary discharge lamp UV source, a 1/2-m Jarrell-Ash grating spectrometer employing a Hamamatsu R166UH photomultiplier detector, associated signal-conditioning electronics, a Hewlett-Packard 5480B signal averager, and a Honeywell 5600C fm tape system; the system is shown schematically in Fig. 13. The function of each component of the system is described in more detail in Refs. 1 through 3. The spectrometer was operated at a slit width such that the half-width of the triangular slit function was 1.6 Å. Basic to the method is detailed knowledge of the fundamental source characteristics — line positions and intensities and the temperature in the discharge region. Reproducibility of the source intensity distribution, as shown in Fig. 14, was checked at UTRC using its 1.5-m J-Y spectrometer (Ref. 4). UTRC's system utilized matched optics to produce a parallel source beam 1.0 cm in diameter for the absorption measurements.

Data were obtained at UTRC by scanning the spectrum several times and by averaging the spectrum using the Hewlett-Packard 5480B signal averager. The averaged spectrum was then recorded on the fm tape and on an X-Y plotter. A reference spectrum was obtained before and after a test on either of the UTRC calibration sources, and several data points at the different operating conditions given in Section 3.1 were obtained. Typical spectral data for the FGH and the FFB are given in Figs. 15 and 16. Data for the absorption cell* were similar and are not shown here.

Problems with the experimental data included differences in reference spectra obtained before and after a test, possibly due to incomplete purging of the viewing tube and/or window fogging. Additional differences were noted between hot zero (burner on—no seed of NO) and cold zero (burner off). These differences contributed to the optical measurement uncertainty.

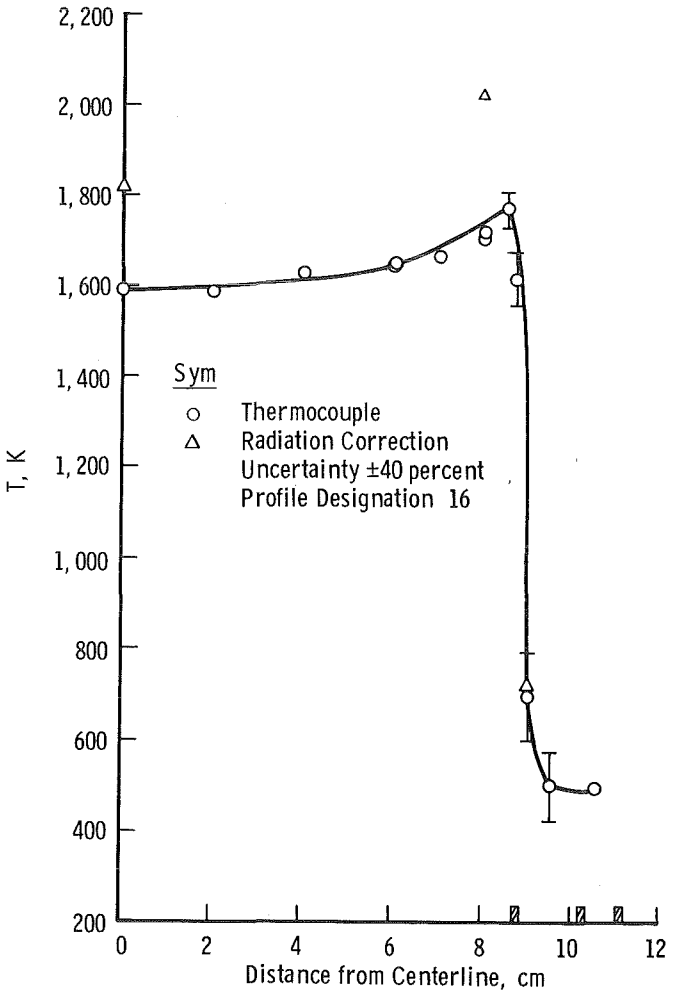

Figure 12. Temperature profile of the flat-flame burner (2,000-K setting).

*The disagreement of these data with the original AEDC model prompted UTRC's investigation of the model and the identification of errors (Ref. 4). The subsequent reexamination of the model by AEDC with the results is presented herein.

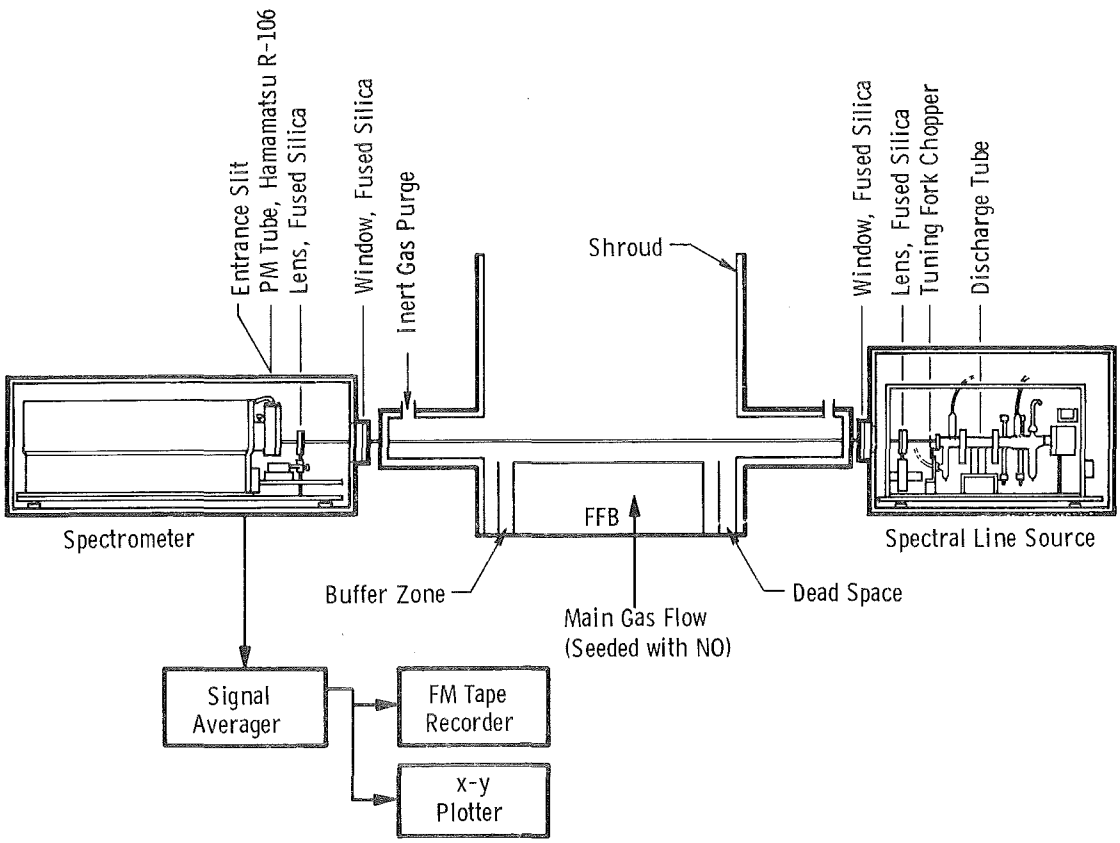

Figure 13. Schematic of AEDC absorption system as used at UTRC.

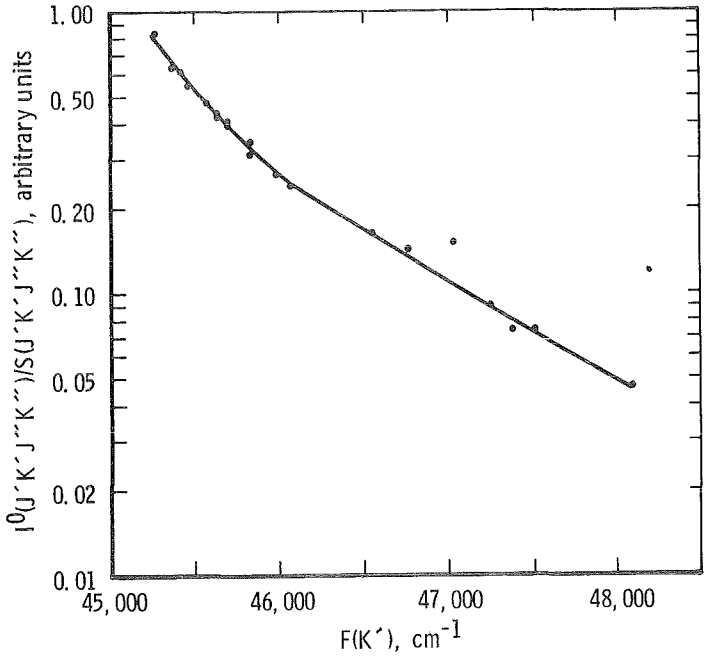

Figure 14. Population distribution of excited rotational states of the $A^2\Sigma$ level of NO in a water-cooled discharge tube operated at 8 torr with 2,800 v applied and containing 12:3:1 mixture (by volume) of $A:N_2:O_2$.

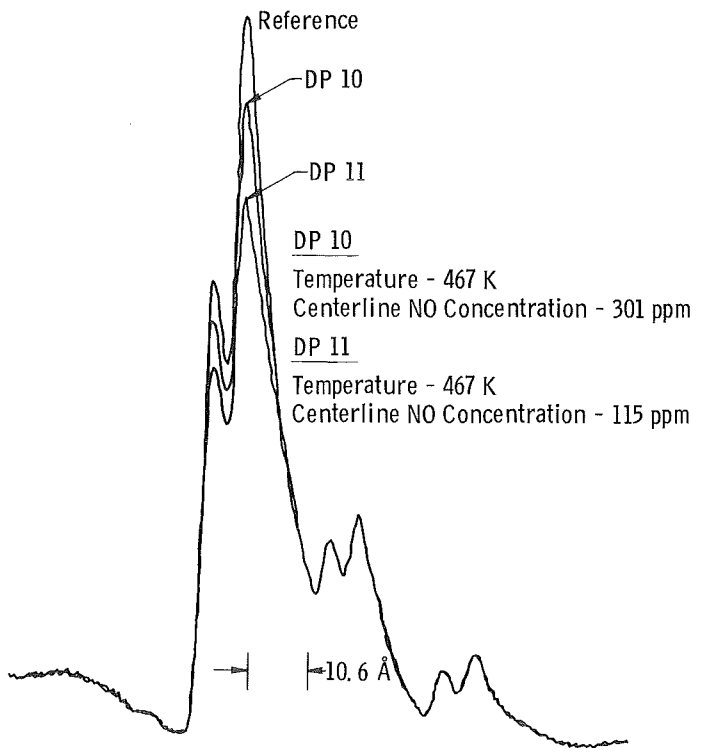

Figure 15. Typical NO (0,0) γ-band absorption spectra from flowing-gas heater.

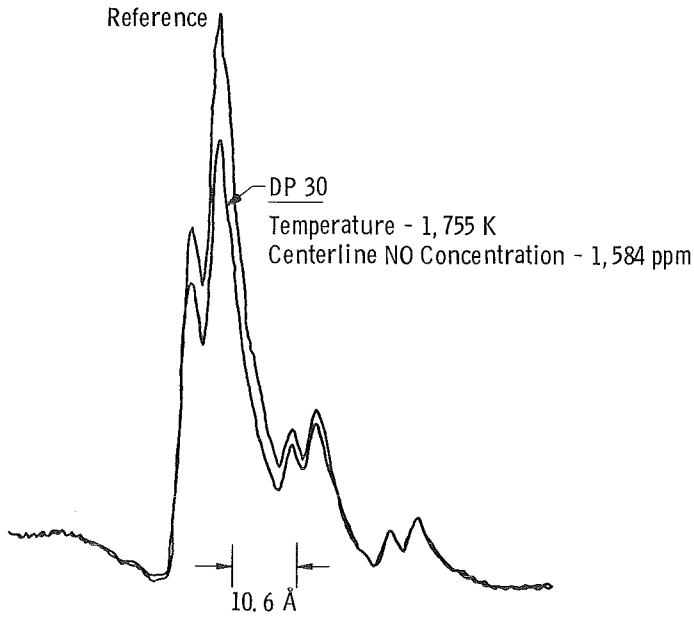

Figure 16. Typical NO (0,0) γ-band absorption spectra from flat-flame burner.

3.3 DATA TREATMENT

3.3.1 Method and Procedure

AEDC's original plan for the absorption data treatment was to employ the iterative radial inversion model of the UV radiative transfer (described in Ref. 2) for a single, homogeneous zone. In that model the NO number density, or concentration, of the homogeneous zone is determined by successive iterations on the NO density until the measured and calculated second bandhead transmittances are the same to within some specified small increment. Since the temperature and concentration were not homogeneous along the FGH or FFB optical paths—as shown by the measured profiles given in section 3.1—this plan was dropped. Instead, it appeared that the best approach to a high-temperature calibration of the model was to compare transmissivities calculated using the measured temperature and NO concentration profiles and to break the path up into several homogeneous zones for which averaged temperatures and NO concentrations had been assigned.

The radiative transfer of line radiation along nonhomogeneous paths is complicated by the changing line shape along the path. This problem is treated in several classic references, including Goody (Ref. 16). Beer's law, which is sometimes used erroneously for the radiative transfer, state that the monochromatic absorption coefficients of zones of different properties are additive. Sometimes the integrated line transmittances are treated, erroneously, as the product of transmittances of the different zones. This procedure is valid only if the source line is much narrower than the absorption lines.

The procedure used here for the radiative transfer calculation is illustrated in Fig. 17 and is detailed for a single line, j, by

$$t_j(\nu) = I^0_{0j}(\nu) \exp\left[\sum_{\ell=1}^{L} -\Delta x_\ell \sum_i k_{i\ell}\left(\nu, T_\ell, p_\ell, n_\ell\right)\right] \tag{15}$$

$$t_j = \int_{\Delta\nu} T_j(\nu)\,d\nu \tag{16}$$

Expressed in words, Eqs. (15) and (16) state that the intensity of the transmitted line, t_j, at the right (receiver) side of the nonhomogeneous path made up of zones of constant properties is calculated by starting the calculation on the left (source) side (see Fig. 17) and determining the frequency function in Eq. 15 for the first zone by breaking the line shape up into a sufficient number of monochromatic points to define the line shape (e.g., 100

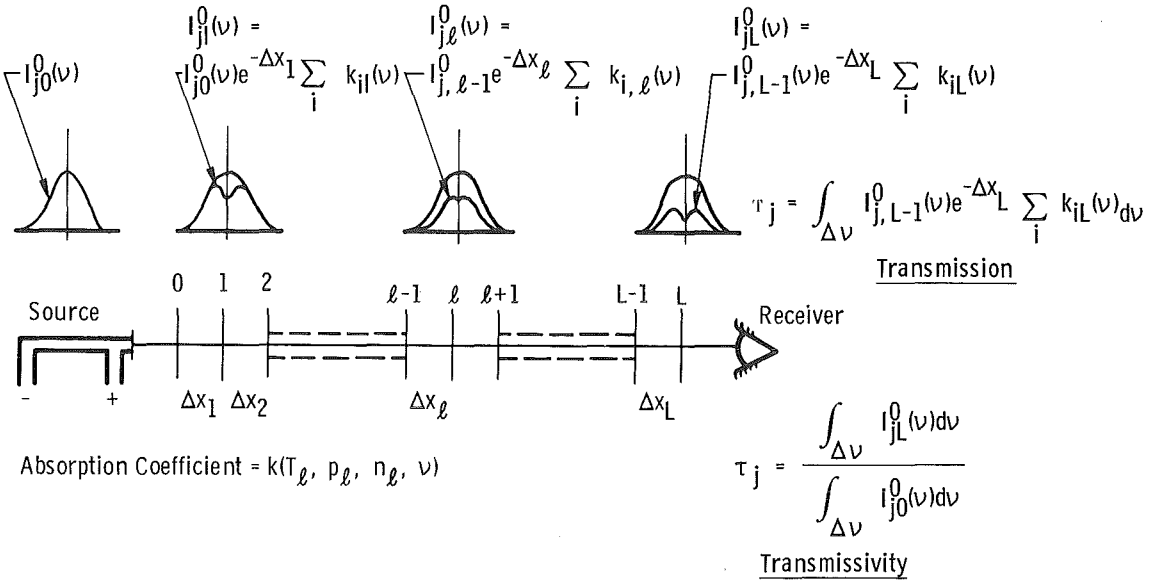

Figure 17. Illustration of spectral line radiative transfer through nongomogeneous media.

frequency points were used for the calculations reported). The result is a new line profile, $I_{j1}(\nu)$, to be used for zone 2, in which the absorption coefficients for all the lines, i, contributing to absorption of source line, j, are determined by the temperature, T_2, pressure, p_2, and NO density, n_2, in zone 2. The result of the zone 2 calculation is the source line profile to be used for zone 3; the zone 3 calculation is used for zone 4 and so forth. At the right boundary of the path, the final shape of the transmitted profile, $t_j(\nu)$, has been determined, and the transmitted intensity integral, t_j [Eq. (16)], is evaluated. The integral transmission values are stored for each line; the computer program that sums the contributions of each line within the instrument bandpass is then run. The line shapes shown in Fig. 17 are exaggerated to emphasize the problem. The shapes represent the effect of a cold boundary with a line width smaller than the source lien width and with subsequent broad lines corresponding to a high-temperature path. Such a situation would be encountered for a jet engine exhaust under altitude conditions.

The revised AEDC model described in Section 2.0 was used along with the above-described radiative transfer model to calculate transmissivities at the second bandhead expected for the FGH and FFB property profiles given in Section 3.1. The 23 zones used are shown in Fig. 18. Local values of the broadening parameter, $\mathfrak{A}$, were computed using Eq. (14) to determine the broadening coefficient.

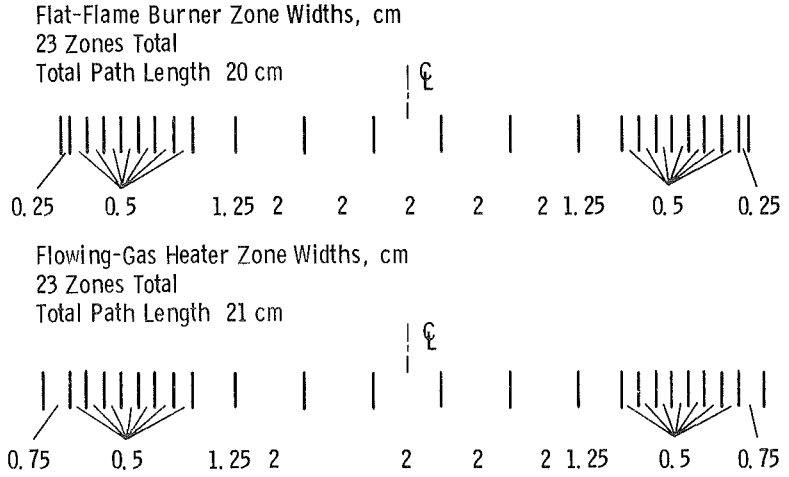

Figure 18. Diagram of zone widths for computer calculation of transmission for the flowing-gas heater and flat-flame burner.

3.3.2 Results

The computed values of the second bandhead transmittance for the absorption cell, the FGH, and the FFB are given in Tables 3, 4, and 5, respectively; the procedure described in the preceding paragraph was used with the temperature and NO concentration profiles given in Section 3.1. The centerline values of concentration listed in Tables 1 and 2 were used, and a uniform pressure of 1 atm was assumed. For several of the data points, profiles as measured by probes were not supplied, and the profiles shown by the solid curves in Figs. 4 through 12 were used.

The transformation of the differences in measured and calculated second bandhead transmissivity to expected differences in NO concentration was computed by the procedure suggested by UTRC (Ref. 4), using the following equation:

$$\text{percent } [\text{NO}] \text{ difference} = \left(\frac{\ell n\, \tau_{meas}}{\ell n\, \tau_{cal}} - 1 \right) 100 \tag{17}$$

The results of this calculation are also shown in Tables 3, 4, and 5. Such an expression may serve as a basis for comparison but cannot be interpreted as a very good estimate of error since it applies only to single lines in the narrow source line limit and to a homogeneous path. Another approach was taken by AEDC for a few data points, the results of which are shown in Table 5. In this approach, the centerline concentration was varied and the

transmittance calculation performed several times until a fit with the measured transmittance was effected. This AEDC method gave differences in predicted and measured transmittance usually about five percent less than those obtained using Eq. (17).

Table 3. Results of Optical Transmission Measurements Made Through Absorption Cell (293 K)

Data Point Number	Pressure, atm	NO Concentration, c, ppm	Transmissivity, τ, measured	Transmissivity, τ, model	$\Delta\tau^*$	Δc^{**}, percent
1	1.0	458	0.482	0.454	0.028	-7.5
2	1.0	93	0.835	0.842	0.007	4.8
3	0.0395	2,080	0.673	0.627	0.046	-15.1
4	1.0	250	0.659	0.637	0.022	-7.5

$$*\Delta\tau = \tau_{model} - \tau_{meas}$$

$$\Delta c = \left(\frac{\ell n\ \tau_{meas}}{\ell n\ \tau_{model}} - 1 \right) 100 \text{ percent}$$

Table 4. Results of Optical Transmission Measurements Made Through Flowing-Gas Heater

Data Point Number	Centerline NO Concentration, c, ppm	Transmissivity, τ, measured	Transmissivity, τ, model	$\Delta\tau^*$	Δc^{**}, percent
2	115	0.836	0.826	-0.010	-6.3
8	115	0.862	0.834	-0.028	-18.2
8	112 (p)	0.862	0.838	-0.024	-16.0
9	301	0.686	0.634	-0.052	-17.3
9	287 (p)	0.686	0.646	-0.640	-13.8
11	115	0.881	0.906	0.025	28.4
12	301	0.743	0.775	0.032	16.5
14	115	0.898	0.908	0.010	11.5
15	301	0.748	0.776	0.028	14.5
17	301	0.731	0.762	0.031	15.3
19	115	0.952	0.953	0.001	2.2
19	105 (p)	0.952	0.957	0.003	11.9
20	301	0.879	0.876	-0.003	-2.6
20	280 (p)	0.879	0.884	0.005	3.7
23	115	0.923	0.947	0.024	47.1
24	301	0.840	0.869	0.029	24.2
27	535	0.762	0.793	0.031	17.2
27	520 (p)	0.762	0.798	0.036	20.5
28	448	0.812	0.831	0.019	12.5
28	430 (p)	0.812	0.837	0.025	14.7

(p) - probe value

$$*\Delta\tau = \tau_{model} - \tau_{meas}$$

$$\Delta c = \left(\frac{\ell n\ \tau_{meas}}{\ell n\ \tau_{model}} - 1 \right) 100 \text{ percent}$$

Table 5. Results of Optical Transmission Measurements Made Through Flat-Flame Burner.

Data Point Number	Centerline NO Concentration, c, ppm	Transmissivity, τ, measured	Transmissivity, τ, model	Δτ*	Δc**, percent	Δc†, percent
7	1,390	0.824	0.854	0.030	22.7	---
7	1,427 (p)	0.824	0.851	0.027	20.0	---
10	1,394	0.607	0.587	-0.020	-6.3	---
10	1,486 (p)	0.607	0.567	-0.040	-12.0	---
13	1,362	0.728	0.759	0.031	14.6	---
13	1,459	0.728	0.744	0.016	7.4	---
16	1,076	0.674	0.661	-0.014	-4.7	---
17	686	0.790	0.766	-0.024	-11.6	---
20	1,052	0.746	0.807	0.061	36.7	---
20	1,119 (p)	0.746	0.796	0.050	28.4	---
21	670	0.832	0.872	0.040	34.3	---
24	1,000	0.817	0.851	0.034	25.4	23.0
24	1,107 (p)	0.817	0.837	0.020	13.4	12.9
25	1,141	0.792	0.832	0.040	26.9	23.5
26	750	0.861	0.886	0.025	23.4	20.6
27	607	0.896	0.906	0.010	11.2	7.6
30	1,584	0.779	0.836	0.057	39.4	---
30	1,671 (p)	0.779	0.828	0.049	32.3	---
33	301	0.578	0.583	0.005	1.6	---
34	214	0.638	0.676	0.038	14.8	---
35	115	0.798	0.806	0.008	4.0	---

(p) - probe value

$*\Delta\tau = \tau_{model} - \tau_{meas}$

$$\Delta c = \left(\frac{\ell n\ \tau_{meas}}{\ell n\ \tau_{model}} - 1 \right) 100 \text{ percent}$$

† determined by matching centerline concentration to fit model.

3.3.3 Discussion

The uncertainties introduced by the nonhomogeneous profiles of temperature and concentration in the FGH and FFB into the "calibration" of the NO UV absorption method at high temperatures made the calibration somewhat less than ideal. In fact, by judicious choice of profiles on most of the data points, the measured and calculated transmittances could be made to agree. For example, the uncertainty in the radiation correction to the temperature for the FFB always permits the transmissivity to be matched by suitable choice of temperature within the error bounds. It should be noted that the preponderence of the data indicates an over-prediction of the NO concentration (over-prediction of the transmittance). Taken overall, the root-mean-square average of the departure of the calculated NO concentration using Eq. (16) is as follows:

Absorption cell	9 percent
Flowing-gas heater	18 percent
Flat-flame burner	21 percent

These results are considered satisfactory, considering the uncertainties in the profiles of temperature and concentration.

Although it represents the correct physics, the radiative transfer calculational procedure introduced here would not be expected to be very different from a Beer's law treatment since the absorption line widths in these experiments were considerably larger than the source line width (i.e., from about 2 to 4). However, for applications to turbine engine exhausts at altitude conditions, the Beer's law procedure would be expected to be considerably in error.

4.0 SUMMARY OF RESULTS

The results obtained by AEDC in Phase 1 of the Interagency NO Measurement Investigation are summarized as follows:

1. Transmissivity measurements of the NO (0,0) γ band were made at the United Technology Research Center laboratories using the calibration cells—room-temperature absorption cell, flowing-gas heater (293 to 833 K), and flat-flame burner (230 to 1,755 K). NO concentration and temperature profile data obtained on the flowing-gas heater and flat-flame burner by UTRC using probe methods were supplied. These data indicated nonhomogeneities which complicated the calibration procedure established for a homogeneous path.

2. UTRC personnel discovered errors in the NO resonance line, radiative transfer model developed at AEDC; AEDC made the necessary revisions, which required a redetermination of parameters. The completed model redevelopment produced a much-improved model and more reliable parameters. (Independently, UTRC also developed a revised model, different in detail but substantially the same as the revised AEDC model, and also acquired moderately high resolution line data and determined an independent set of parameters.)

3. The newly obtained broadening cross sections are approximately equal for N_2, A, and CO_2 (about $547 \pm 53 \times 10^{-16}$ cm^2). Broadening by H_2O (for which experimental data are difficult to obtain) and O_2 were assumed to have the same cross section as N_2, A, and CO_2. This is important for the H_2/O_2 flat-flame burner used by UTRC in which as much as 40 percent of the effluent volume is H_2O. This assumption results in added uncertainty in the calculated transmissivities.

4. A radiative transfer calculation procedure for spectral lines transmitted through nonhomogeneous media was developed and applied to the data obtained at UTRC by AEDC. The procedure avoids incorrect applications in the assumptions of Beer's law, which are reasonable for this data where the absorber

line half-widths are considerably greater than the source line half-widths. Serious difficulty with the Beer's law assumption would be expected for sources such as turbine engine exhausts at simulated altitudes.

5. The calibration results for the AEDC system from Phase 1 of the Interagency program, though not ideal because of the nonhomogeneity of the paths and because of the uncertain temperature and concentration profiles in the calibration devices, were deemed satisfactory. An average prediction of about 20-percent uncertainty in NO concentration can be made using the AEDC UV resonance line absorption technique, based upon these results.

REFERENCES

1. Few, J. D., Bryson, R. J., and McGregor, W. K. "Evaluation of Probe Sampling versus Optical In Situ Measurements of Nitric Oxide Concentrations in a Jet Engine Combustor Exhaust." AEDC-TR-76-180 (ADA034726), September 1971.

2. Few, J. D., McGregor, W. K., and Glassman, H. N. "Comparison of UV Absorption Measurements with Probe-Sampling Measurements of Nitric Oxide Concentrations in a Jet Engine Combustor Exhaust." AEDC-TR-76-134 (ADA030005), September 1976.

3. Few, J. D. "Optical Measurement of NO and NO_2 in the Exhaust of an F101-GE-100 Engine at Simulated Altitudes." AEDC-TR-77-75 (AD-A047882), December 1977.

4. Dodge, L. G., Colket, M. B., III, Zabielski, M. F., Dusek, J., and Seery, D. J. "Nitric Oxide Measurement Study: Optical Calibration." DOT-FAA Contract No. FA77WA-4081. (In review.)

5. Davis, M. G., McGregor, W. K., Few, J. D., and Glassman, H. N. "Transmission of Doppler Broadened Resonance Radiation Through Absorbing Media with Combined Doppler and Pressure Broadening (Nitric Oxide γ-Bands as an Example)." AEDC-TR-76-12 (ADA021061), February 1976.

6. Herzberg, G. *Spectra of Diatomic Molecules.* D. Van Nostrand Co., New York, 1950.

7. Tatum, J. B. *Astrophysical Journal.* Supplement Series. Vol. 14, Supplement No. 124, 1967.

8. Pery-Thorne, A. and Banfield, F. G. "Absolute Oscillator Strength of the (0,0) Band of the Gamma System of Nitric Oxide by the Hook Method." *Journal of Physics. B: Atomic and Molecular Physics*, Vol. 3, No. 7, July 1970, pp. 1011-1019.

9. Keefer, D. R. "Level Populations for Molecules Intermediate to Hund's Cases (a) and (b): The NO $X^2\Pi$ State as an Example." (Submitted to *Journal of Quantitative Spectroscopy and Radiative Transfer.*)

10. Penner, S. S. *Quantitative Molecular Spectroscopy and Gas Emissivities.* Addison-Wesley Co., Reading, Mass., 1959.

11. Deeszi, I. *Acta Physica.* Vol. 9

12. Engleman, R., Jr., Rouse, P. E., Peck, H. M., and Baiamonte, V. D. "Beta and Gamma Systems for Nitric Oxide." Los Alamos Report LA-4364, Los Alamos Scientific Laboratory, University of California, New Mexico, July 1970.

13. Hasson, V., Farmer, A. J. D., Nicholls, R. W., and Anketell, J. "Application of Dispersion Techniques to Molecular Band Intensity Measurements. II: Oscillator Strength of the (0,0) Band of NO-γ ($A^2\Sigma$-$X^3\Pi$) System." *Journal of Physics. B: Atomic and Molecular Physics*, Vol. 5, No. 6, June 1972, pp. 1248-1254.

14. Farmer, A. J. D., Hasson, V., and Nicholls, R. W. "Absolute Oscillator Strength Measurements of the ($v'' = 0$, $v' = 0$-3) Bands of the ($A^2\Sigma$-$X^2\Pi$) γ-System of Nitric Oxide." *Journal of Quantitative Spectroscopy and Radiative Transfer*, Vol. 12, No. 4, April 1972, pp. 627-633.

15. Benson, R. and Samuelson, G. S. "Oxides of Nitrogen Transformation While Sampling Combustion Products Containing Carbon Monoxide and Hydrogen." Presented at Combustion Institute, Fall Meeting, LaJolla, California, October 18-20, 1976. Paper 76-39.

16. Goody, R. M. *Atmospheric Radiation. I: Theoretical Basis.* Clarendon Press, Oxford, 1964.

17. Mitchell, A. C. G. and Zemansky, M. W. *Resonance Radiation and Excited Atoms.* Cambridge University Press, London, 1971.

18. Present, R. D. *Kinetic Theory of Gases.* McGraw-Hill, New York, 1958.

APPENDIX A
DERIVATION OF COLLISIONAL BROADENING RELATIONS

Some confusion exists in the literature in regard to the origin of expressions for collisional "half-widths," "optical collision diameters," and "optical cross sections." This appendix is intended to clarify these expressions as they are used in this report.

The full width at half-maximum, $(\Delta\nu)_L$, of a collision-broadened spectral line is defined as Z_L/π, where Z_L is the number of collisions per unit time per atom giving rise to the broadening of a line (Ref. 17). The Lorentz frequency function is classically used to describe the shape, $b_L(\nu)$, of a natural or collision-broadened line,

$$b_L(\nu) = \frac{\text{constant } (\Delta\nu)_L^2}{(\Delta\nu)_L^2 + (\nu - \nu^0)^2} \tag{A-1}$$

where ν^0 is the frequency at line center. Now, if the concepts of kinetic theory are used, the mean collision frequency between two molecules, a and b, per number of molecules, a, is given by

$$\left[(\Delta\nu)_L\right]_{ab}^{-1} = Z_{ab} = \left(\pi d_{ab}^2\right) n_b \, v_{ab} \tag{A-2}$$

where n_b is the number density of molecules, b; v_{ab} is the mean speed between the molecules; and d_{ab} is the diameter of the sphere of influence between the molecules involved in the collision. Thus, πd_{ab}^2 is an area which may be designated as a "cross section" for the collision, σ_{ab}. The "optical collisional diameter" for broadening is defined as d_{ab}. Both terms are in reality unknown and are directly related to the probability that a collision promotes a departure from the stationary state probability of transition. The mean speed for molecules having a Maxwell-Boltzmann velocity distribution function is (Ref. 18)

$$\bar{v}_{ab} = \left(\frac{8\kappa T}{\pi M_{ab}}\right)^{1/2} = 2\left(\frac{2\kappa T}{\pi}\right)^{1/2}\left(\frac{1}{M_a} + \frac{1}{M_b}\right)^{1/2} \tag{A-3}$$

where $\varkappa$ is Boltzmann's constant, T is the temperature, M_{ab} is the the reduced mass, and M_a and M_b are the masses of the molecules a and b, respectively. The density of molecules, b, is given by

$$n_b = \frac{f_b p}{\kappa T} \tag{A-4}$$

where p is the pressure of the gas mixture and f_b is the mole fraction of molecules, b. Combining Eqs. (A-2) through (A-4) results in the following:

$$\left[(\Delta\nu)_L\right]_{ab} = \frac{2}{\pi} p \left(\frac{2}{\pi\kappa T}\right)^{1/2} \sigma_{ab} f_b \left(\frac{1}{M_a} + \frac{1}{M_b}\right)^{1/2} \tag{A-5}$$

If more than one molecule b contributes to the broadening of spectral lines emitted or absorbed by molecule a, then

$$\left[(\Delta\nu)_L\right]_a = \frac{2}{\pi} p \left(\frac{2}{\pi\kappa T}\right)^{1/2} \sum_b \sigma_{ab} f_b \left(\frac{1}{M_a} + \frac{1}{M_b}\right)^{1/2} \tag{A-6}$$

If the lines are also broadened by the Doppler effect, the line shape is given by the Voigt profile (Ref. 17):

$$b_\nu(\nu) = \frac{1}{\pi} \int_{-\infty}^{\infty} \frac{\mathfrak{a} e^{-y^2}}{\mathfrak{a}^2 + (\omega - y)^2} \, dy \tag{A-7}$$

where y is a variable of integration, ω is the Doppler function

$$\omega = 2\sqrt{\ell n\, 2} \; \frac{\nu - \nu^0}{(\Delta\nu)_D} \tag{A-8}$$

with ν^0 the line center frequency and $(\Delta\nu)_D$ is the full width at half-maximum of the Doppler line shape function. The latter is given by

$$b_D(\nu) = e^{-\omega^2} \tag{A-9}$$

and the Doppler half-width is (Ref. 17)

$$(\Delta\nu)_D = 2\nu^0 \sqrt{\frac{2\,\ell n\,2\,\kappa T}{M_a c^2}} \tag{A-10}$$

where c is the velocity of light. The parameter $\mathfrak{A}$ in Eq. (A-7) is the "collisional broadening parameter" and is defined as

$$\mathfrak{A} = \sqrt{\ell n\,2}\,\frac{(\Delta\nu)_L}{(\Delta\nu)_D} \tag{A-11}$$

Now, inserting Eqs. (A-6) and (A-10) into (A-11) and putting $\nu^0 = c/\lambda$ where λ is the wavelength of the line give the following:

$$\mathfrak{A} = \frac{\lambda}{\kappa\pi^{3/2}} \sum_b f_b \sigma_{ab} \left(1 + \frac{M_a}{M_b}\right)^{1/2} \frac{p}{T} \tag{A-12}$$

or

$$\mathfrak{A} = C\,\frac{p}{T} \tag{A-13}$$

where C is the "collision-broadening coefficient" defined as

$$C = \frac{\lambda}{\kappa \pi^{3/2}} \sum_b f_b \sigma_{ab} \left(1 + \frac{M_a}{M_b}\right)^{1/2} \tag{A-14}$$

In terms of the "optical collision diameter" Eq. (A-14) becomes

$$C = \frac{\lambda}{\kappa \sqrt{\pi}} \sum_b f_b d_{ab}^2 \left(1 + \frac{M_a}{M_b}\right)^{1/2} \tag{A-15}$$